Analytical and Numerical Techniques for Analyzing an Electrically Short Dipole with a Nonlinear Load

MOTOHISA KANDA, MEMBER, IEEE

Abstract—**An electrically short dipole with a nonlinear dipole load is analyzed theoretically using both analytical and numerical techniques. The analytical solution is given in terms of the Anger function of imaginary order and imaginary argument and is derived from the nonlinear differential equation for the Thévenin's equivalent circuit of a dipole with a diode. The numerical technique is to solve the nodal equation using a time-stepping finite difference equation method. The nonlinear resistance of the diode is treated using the Newton–Raphson iteration technique. A comparison between the analytical and numerical solutions is given.**

I. INTRODUCTION

IT IS WELL accepted that microwave radiation can produce biological effects. Although it is very difficult to determine the biological hazards associated with electromagnetic (EM) fields, the biological effects resulting from the EM fields can be adequately described from the knowledge of one or more parameters that characterize the EM field. One of the advocated field parameters for quantifying hazardous EM fields is an electric energy density which can be easily calculated from the electric field strength [1]. For this reason the National Bureau of Standards has recently developed a broadband isotropic electric energy density meter (EDM). The EDM consists of three orthogonal electrically short dipoles with diode detectors between the arms of the dipoles. To synthesize such an EDM in terms of its frequency response and its dynamic range one needs to theoretically analyze an electrically short dipole with a nonlinear load such as a diode.

Traditionally, the characteristics of an antenna with a nonlinear load have been analyzed in the frequency domain by considering the spectral components of the solutions at harmonic frequencies [2]. For example, Sarkar and Weiner [3] have used the Volterra series analysis to obtain the scattering due to nonlinearly loaded antennas. The nonlinear transfer function of a nonlinearly loaded antenna was determined at several harmonic frequencies. The calculation of the nonlinear transfer function is generally tedious, particularly when the circuit model of the nonlinear load is complicated and its nonlinearity is strong. Recent analyses of nonlinearly loaded antennas have been considered using direct time-domain techniques. Schuman [4] has described the application of the time-domain method of moments technique to determine the scattering current on a thin wire with discrete nonlinear resistive loading. Liu and Tesche [5], [6] have used frequency-domain data to compute the time-dependent currents and voltages across a nonlinear load by means of the Laplace transform. A unified numerical procedure was recently proposed by Landt [7]. The antenna characteristics were derived from a time-domain electric field integral equation, whereas the nonlinear network analysis was performed in a simple time-domain nodal analysis.

Two techniques for analyzing an electrically short dipole with a nonlinear load are described here. The first technique, described in Section II-A, gives an analytical solution to the first-order nonlinear time-domain differential equation in terms of Anger functions. The second technique, described in Section II-B, is a time-stepping finite difference solution technique for obtaining a numerical solution to the time-domain nonlinear differential equation. The nonlinear effect due to a diode is solved by the Newton–Raphson iteration method. This numerical technique gives the physical insight for nonlinear load effects on antennas in terms of the time-domain waveform and also permits the consideration of certain problems which are too complicated to be treated by an analytical technique.

The nonlinear effects on an electrically short dipole are first investigated in Section III in the time domain using a time-stepping finite difference solution technique. The frequency responses and the dynamic ranges of the dipole with a nonlinear diode are then compared using the two different techniques described above.

II. THEORY

Using the frequency-domain concept of the effective length and the driving point impedance of an electrically short dipole without a nonlinear load, the Thévenin's equivalent circuit for a diode with a nonlinear load is shown in Fig. 1. The element $v_i(t)$ is the induced open-circuit voltage at the dipole terminal and is given by

$$v_i(t) = e_{\text{inc}}(t) h_e, \tag{1}$$

where e_{inc} is the normal incident electric field strength and h_e is the effective length of the dipole. The element C_a is the equivalent driving point capacitance of the dipole. A parallel combination of a linear capacitance C_d and a nonlinear resistance R_d represents a simplified model of a diode.

For an electrically short dipole antenna (i.e., $kh < 1$ where k is the free-space wavenumber), the effective length h_e and the driving point capacitance C_a of an antenna are given by [8]

$$h_e = \frac{h(\Omega - 1)}{2(\Omega - 2 + \ln 4)} \quad \text{m}, \tag{2}$$

and

$$C_a = \frac{4\pi\epsilon_0 h}{(\Omega - 2 - \ln 4)} \quad \text{F}. \tag{3}$$

The symbols have the following meanings: h is half the physical length of a dipole antenna in meters, ϵ_0 is the free-space

Manuscript received November 13, 1978; revised August 1, 1979.

The author is with the Electromagnetic Fields Division, National Bureau of Standards, Boulder, CO 80303.

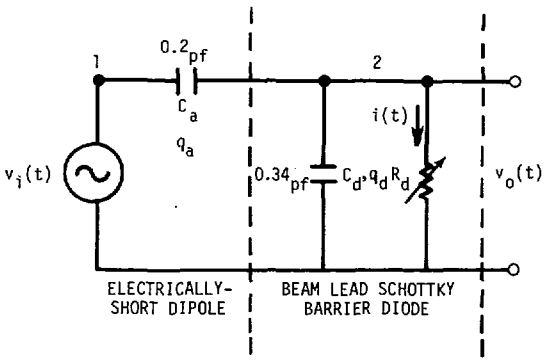

Fig. 1. Thévenin's equivalent circuit of an electrically short dipole with a diode.

permittivity in farads/meter, and Ω is the antenna thickness factor (i.e., $\Omega = 2\ ln(2h/a)$, where a is the antenna radius in meters). When $h = 0.02$ m and $a = 2.84 \times 10^{-5}$ m (i.e., the antenna thickness factor $\Omega = 14.50$), the effective length h_e and the equivalent antenna input capacitance of the antenna C_a become, respectively, 9.72×10^{-3} m and 0.2×10^{-12} F.

A beam lead Schottky barrier diode is chosen as a nonlinear load detector since it has a natural high-frequency performance due to small junction capacitance, high sensitivity, and low noise characteristics. When an electrically short dipole is terminated with a beam lead Schottky barrier diode, the effect of loading on an antenna can be analyzed using the simple equivalent circuit shown in Fig. 1, which consists of a parallel combination of a nonlinear resistance R_d and a linear capacitance C_d. Here, the nonlinear resistance R_d of the diode is characterized by its v-i characteristic, i.e.,

$$i(t) = I_s(e^{\alpha v_0(t)} - 1). \tag{4}$$

The symbols have the following meanings: $i(t)$ is the current (ampere) and $v_0(t)$ is the voltage (volt) across the diode junction; I_s is the saturation current which is assumed to be 2×10^{-9} A; and $\alpha = q/nkT \cong 38\ V^{-1}$, where q is the electronic charge (1.6×10^{-19} C), n is the diode ideality factor ($\sim$1.05), k is Boltzmann's constant (1.38×10^{-23} J/K), and T is the temperature ($\sim$290 K).

The junction capacitance C_j and the package capacitance C_p are combined and are shown as C_d in Fig. 1. The exact value of C_d varies from diode to diode and is very difficult to determine. In this paper, C_d is assumed to be constant and equal to 0.34 pF for a beam lead Schottky barrier diode. In a more elaborate diode model the junction capacitance C_j is nonlinear and is a function of the built-in potential V_b as

$$C_j(V) = \frac{C_j(0)}{\left(1 - \dfrac{V}{V_b}\right)^{1/2}} \tag{5}$$

for a step junction. The package capacitance C_p is generally constant. The more general treatment of an antenna with linear and nonlinear loads, such as a nonlinear resistance and a nonlinear junction capacitance as well as a linear package inductance and a linear series resistance of a diode, is being pursued. A simple nonlinear resistance R_d with a constant diode capacitance C_d for the beam lead Schottky barrier diode shown in Fig. 1 is used in the following sections for analyzing the loading effect of an electrically short dipole with a nonlinear diode using analytical and numerical techniques.

A. Analytical Technique

Using Thévenin's equivalent nonlinear circuit shown in Fig. 1, the voltage equation and the corresponding current equation are

$$v_i(t) + \frac{q_a(t)}{C_a} = \frac{q_d(t)}{C_d} = v_0(t) \tag{6}$$

and

$$\frac{dq_a(t)}{dt} + \frac{dq_d(t)}{dt} + i(t) = 0, \tag{7}$$

where q_a and q_d are the charges on C_a and C_d, respectively, and i is the current through the nonlinear resistance R_d. With the substitution

$$y(t) = e^{\alpha v_0(t)}, \tag{8}$$

(4), (6), and (7) reduce to

$$\frac{dy(t)}{dt} + ay^2(t) + y(t)f(t) = 0, \tag{9}$$

where

$$a = \frac{\alpha I_s}{C_a + C_d}, \tag{10}$$

$$f(t) = \frac{-\alpha}{(1 + C_d/C_a)} \left[\frac{I_s}{C_a} + \frac{dv_i(t)}{dt}\right]. \tag{11}$$

Equation (9) is a first-order nonlinear differential equation. The original investigations for solving the equation have been performed by P. F. Wacker, and the detailed mathematical steps involved are given in Appendix A. When the induced voltage $v_i(t)$ is a periodic sinusoid, i.e., $v_i(t) = V_i \sin \omega t$, the detected dc voltage $\bar{V}_0$ averaged over a complete cycle is given by

$$\bar{V}_0 = -\frac{1}{\alpha} \ln \frac{\pi T J_{jT}(jU)}{\sinh \pi T}, \tag{12}$$

where $J_{jT}(jU)$ is the Anger function of imaginary order (jT) and imaginary argument (jU), T is the normalized period

$$T = \frac{\alpha I_s}{\omega(C_a + C_d)}, \tag{13}$$

and U is the normalized induced voltage

$$U = \frac{\alpha V_i}{1 + C_d/C_a}. \tag{14}$$

Using the series representation for the Anger function one can show from Appendix B that the detected dc voltage averaged over a complete cycle is given by

$$\bar{V}_0 = -\frac{1}{\alpha} \ln [S_1(T, U) - TS_2(T, U)], \tag{15}$$

where

$$S_1(T, U) = 1 + \sum_{\substack{m=2 \\ \text{even}}}^{\infty} \frac{U^m}{\prod_{\substack{k=2 \\ \text{even}}}^{m} (k^2 + T^2)}, \tag{16}$$

and

$$S_2(T, U) = \sum_{\substack{m=1 \\ \text{odd}}}^{\infty} \frac{U^m}{\prod_{\substack{k=1 \\ \text{odd}}}^{m} (k^2 + T^2)}. \tag{17}$$

At high frequencies where

$$T = \frac{\alpha I_s}{\omega(C_a + C_d)} \ll 1, \tag{18}$$

one can show from Appendix C that for small V_i

$$\bar{V}_0 = -\frac{\alpha}{4}\left[\frac{V_i}{1 + C_d/C_a}\right]^2, \tag{19}$$

and for large V_i

$$\bar{V}_0 = -\frac{V_i}{1 + C_d/C_a}. \tag{20}$$

Equation (19) indicates that for the small induced steady-state voltage V_i, the output dc voltage $\bar{V}_0$ is a square-law function of the induced voltage V_i. On the other hand, (20) indicates that for the large induced voltage V_i, the output dc voltage is proportional to the induced voltage V_i.

B. Numerical Technique

A time-stepping difference equation technique can be used for solving the nonlinear network shown in Fig. 1. The basic idea of a time-stepping finite difference equation technique is briefly discussed below. More detailed discussion on this subject is given by Calahan [9].

The linear and nonlinear elements are converted into resistance-current source equivalent networks in the nodal equation method. For instance, in a regular R, C, and L circuit we have

$$v_n = Ri_n, \tag{21}$$

$$i_{n+1} = C\,\frac{v_{n+1} - v_n}{\tau}, \tag{22}$$

and

$$v_{n+1} = L\,\frac{i_{n+1} - i_n}{\tau}, \tag{23}$$

where τ is a sampling time interval. Once the initial v_0 or i_0 is given, one can determine v_1 and i_1, then v_2 and i_2, etc.; such a method is, therefore, called a time-stepping finite difference equation method.

In order to deal with nonlinear equations which result from nonlinear elements such as a diode, the general approach to a solution of such problems is by the Newton–Raphson iteration. The basic technique used is discussed below. Given a nonlinear system $f(i,v)$, the solution of $f(i,v) = 0$ yields the solution for the system response. First $f(i, v)$ is expanded at an initial solution

$$\begin{bmatrix} i^0 \\ v^0 \end{bmatrix},$$

that is,

$$f(i, v) = f(i^0, v^0) + J[f(i^0, v^0)]\begin{bmatrix} \Delta i^0 \\ \Delta v^0 \end{bmatrix}, \tag{24}$$

where J is the Jacobian of f and has the form

$$J = \begin{bmatrix} \dfrac{\partial f_1}{\partial i_1} & \cdots & \dfrac{\partial f_1}{\partial v_{n+m}} \\ \vdots & & \vdots \\ \dfrac{\partial f_{n+m}}{\partial i_1} & \cdots & \dfrac{\partial f_{n+m}}{\partial v_{n+m}} \end{bmatrix}. \tag{25}$$

Now $f(i, v) = 0$ determines

$$\begin{bmatrix} \Delta i^0 \\ \Delta v^0 \end{bmatrix}$$

as

$$J[f(i^0, v^0)]\begin{bmatrix} \Delta i^0 \\ \Delta v^0 \end{bmatrix} = -f(i^0, v^0). \tag{26}$$

The solution of

$$\begin{bmatrix} \Delta i^0 \\ \Delta v^0 \end{bmatrix}$$

updates the initial value of

$$\begin{bmatrix} i^0 \\ v^0 \end{bmatrix},$$

via

$$\begin{bmatrix} i^{n+1} \\ v^{n+1} \end{bmatrix} = \begin{bmatrix} i^n \\ v^n \end{bmatrix} + \begin{bmatrix} \Delta i^n \\ \Delta v^n \end{bmatrix}. \tag{27}$$

The operation is repeated for $n = 0, \cdots$ until the change

$$\begin{bmatrix} \Delta i \\ \Delta v \end{bmatrix}$$

is significantly small.

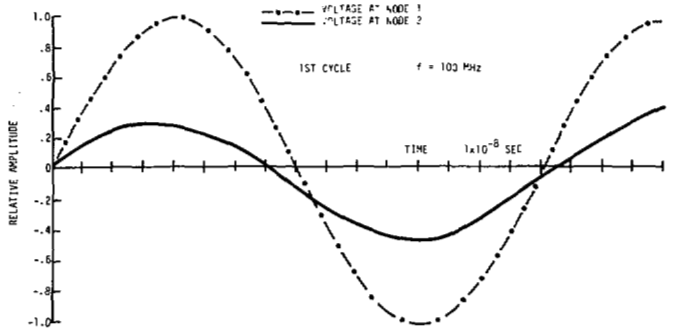

Fig. 2. Time-domain waveform of first detected 100-MHz sinusoid.

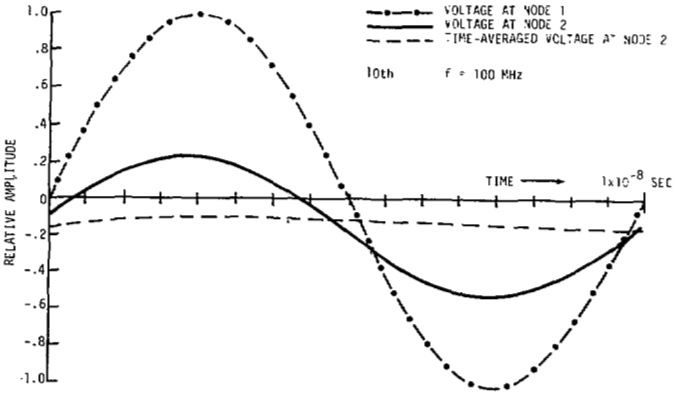

Fig. 3. Time-domain waveform of tenth detected 100-MHz sinusoid.

III. RESULTS

In this section the time-domain waveforms of a sinusoidal wave at various nodes are shown first using the time-stepping difference equation technique discussed in Section II-B. Here a single time-domain sinusoidal wave is divided into 16 discrete digitized points (17 points including both ends) in the analysis. Then the detected sinusoidal wave averaged over many cycles which correspond to dc output of an electrically short dipole with a beam lead Schottky barrier diode is given.

Fig. 2 shows the time-domain waveform of the first sinusoidal wave at 100 MHz at various nodes. At node 1 an applied sinusoidal wave V_i is shown with unit amplitude. At node 2 the detected sinusoidal wave, which is skewed or distorted due to the nonlinearity of the diode, is shown. It is obvious that at node 2 the detected voltage starts developing in the negative polarity, which eventually leads to dc negative output for the dipole with the diode.

Fig. 3 shows the time-domain waveform of the dipole with the diode due to the tenth sinusoidal wave driving voltage. Again, a sinusoidal wave at node 1 is an applied driving votlage with unit amplitude. The detected time-domain waveform at node 2 after diode detection indicates a much more pronounced negative charge accumulation. Finally, an almost dc detected voltage starts appearing in the negative polarity after a ten-cycle time average.

Fig. 4 shows the time-domain waveforms of the dipole with the diode due to the 100th sinusoidal wave induced voltage. The negative charge accumulation is much more pronounced, and constant detected dc voltage appears after a 100-cycle time average. To arrive at the steady-state time average of these sinusoidal wave excitations using the time-stepping finite difference equation technique with the Newton–Raphson iteration method, 400 sinusoidal waves, which correspond to 6400

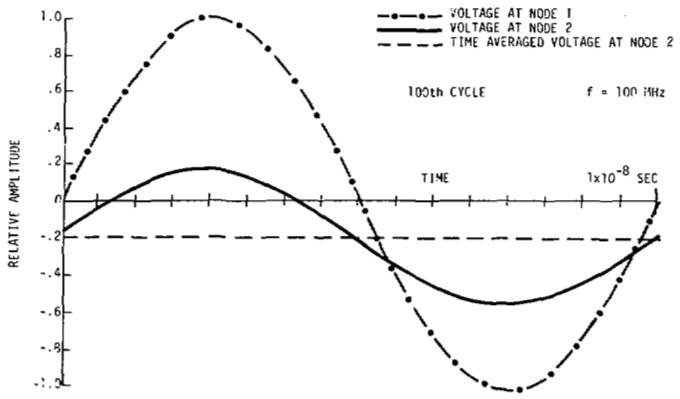

Fig. 4. Time-domain waveform of 100th detected 100-MHz sinusoid.

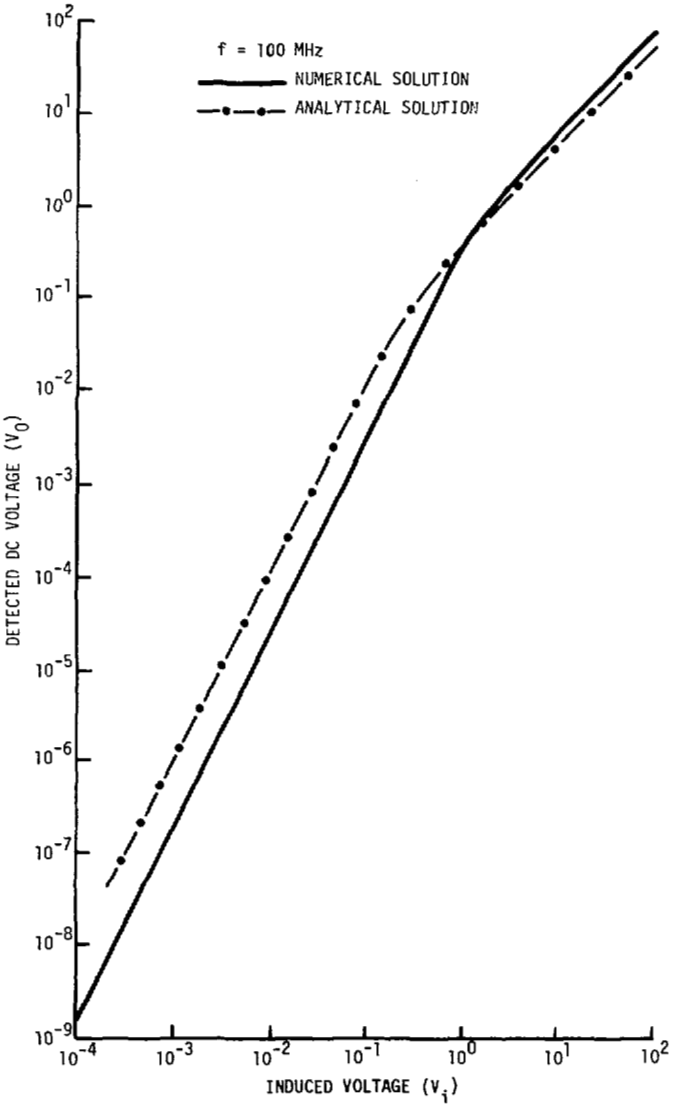

Fig. 5. Detector voltage response at 100 Mhz.

discrete points (16 points per one cycle), are applied successively to compute 6400 discrete output voltages, which are then numerically time-averaged.

Fig. 5 shows the detected dc voltage V_0 from the dipole with the diode as a function of induced voltage $V_i (= e_{inc}\ h_e$, where e_{inc} is the normal incident electric field and h_e is the dipole effective length). The detected dc voltages V_0 as a func-

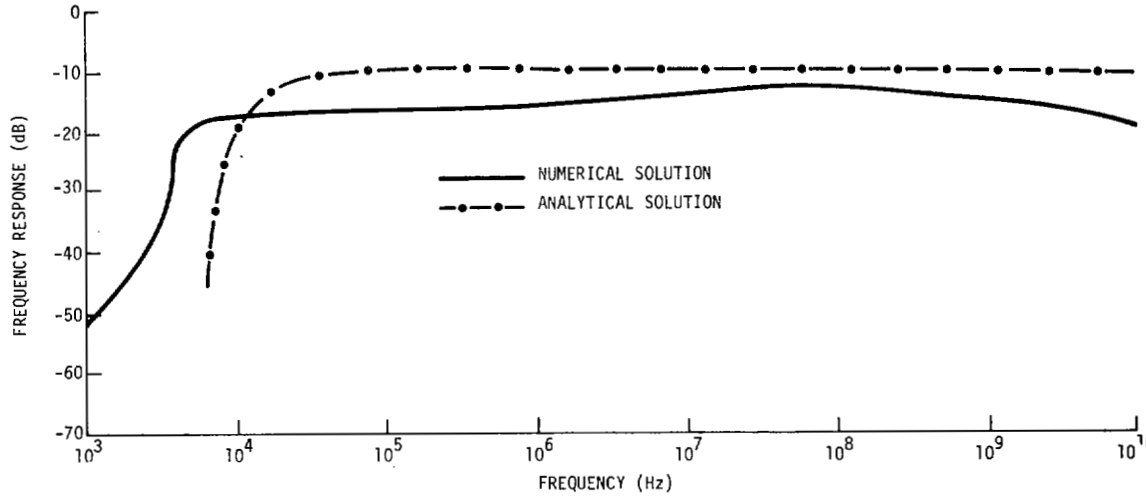

Fig. 6. Transfer function of an electrically short dipole with a nonlinear load.

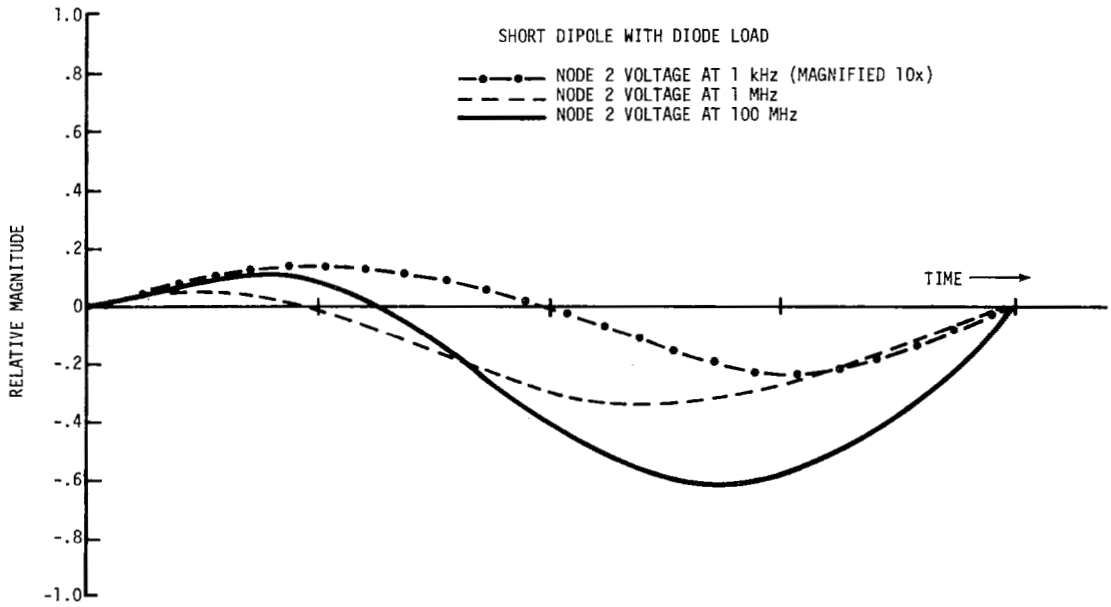

Fig. 7. Time-domain waveform of detected sinusoids at various frequencies.

tion of induced voltage V_i are calculated using both the analytical technique given in Section II-A and the numerical technique described in Section II-B. Below an induced voltage V_i of about one volt, the detected dc voltage $\bar{V}_0$ is equal to the square of the induced voltage V_i. On the other hand, above an induced voltage V_i of about one volt, the detected dc voltage $\bar{V}_0$ is proportional to the induced voltage V_i. Thus the diode detection is square-law at a small signal level but becomes linear at a large signal level.

Fig. 6 shows the transfer function of an electrically short dipole with a beam lead Schottky barrier diode as a function of frequency. Here the transfer function is defined as a ratio of the detected dc voltage $\bar{V}_0$ to the amplitude of the induced voltage $V_i (= e_{inc}\ h_e)$ expressed in decibels when e_{inc} is equal to 1 V/m rms. Thus the transfer function so defined is for a detected dc voltage $\bar{V}_0$ of several millivolts, which corresponds to a square-law signal level. As indicated in (2), the effective length of an electrically short dipole is independent of frequency. The transfer functions of the dipole with the diode are calculated both analytically and numerically.

The sharp cutoff (20 ~ 40 dB per octave) below 10 kHz in the transfer function predicted from both analytical and numerical results can be explained as follows. Fig. 7 shows the detected time-domain sinusoidal waveforms at node 2 at various frequencies. Since the induced voltage V_i becomes very small at low frequencies below 10 kHz, the diode provides a very high and almost linear impedance for both the positive and negative cycles of the sinusoids. Therefore, the detected time-domain sinusoidal waveform becomes very similar to the original sinusoidal wave excitation. For example, Fig. 7 clearly shows that the time-domain waveform at 1 kHz (whose amplitude is magnified by a factor of 10) is almost sinusoidal for both the positive and negative cycles. On the other hand, at high frequencies above 10 kHz, during the positive cycle the diode conducts and provides a very low impedance, whereas during the negative cycle the diode does not conduct and provides a very high impedance. Therefore, the time-domain waveforms at high frequencies above 10 kHz are more skewed or distorted compared with the original sinusoidal waveforms. Fig. 7 clearly shows that the detected time-domain waveforms

at 1 and 100 MHz are more skewed or distorted compared with those at 1 kHz. The detected time-domain sinusoidal waveform is less strongly skewed or distorted at lower frequencies than at higher frequencies. Because the skewness of the detected waveform and the rate of charge accumulation decrease in the lower frequency range below 10 kHz, the transfer function of the dipole with the diode also decreases as shown in Fig. 6.

IV. CONCLUSION

This paper introduces two independent techniques to analyze an electrically short dipole with a nonlinear load. The nonlinear load considered in this paper is a beam lead Shottky barrier diode. The analytical solution, given in Section II-A in terms of the Anger function of imaginary order and imaginary argument, was derived from the nonlinear differential equation for the Thévenin's equivalent of the dipole with the diode. The numerical technique, explained in Section II-B, is basically to solve nodal equations using a time-stepping finite difference equation technique. The nonlinear resistance of a diode was treated by the Newton–Raphson iteration method.

The transition from the square-law detection region to the linear detection region was observed as the induced voltage was varied. The transfer function of an electrically short dipole with a diode was also investigated. The decrease in the transfer function at frequencies below 10 kHz was explained through the time-domain sinusoidal waveforms obtained from a time-stepping finite difference equation technique.

One of the advantages of using the analytical solution in terms of the Anger function of imaginary order and imaginary magnitude is that the solution is given in the closed form and is very easy to evaluate. However, it is very difficult, or maybe even impossible, to find the closed-form solution of a nonlinear differential equation for much more complicated models of an antenna and a diode, e.g., including a nonlinear capacitance, a linear inductance, as well as nonlinear and linear resistances, and a linear capacitance. In such cases a time-stepping finite difference equation technique along with the Newton–Raphson iteration method provides an accurate time-domain solution for more general nodal equations. The analysis of a linear antenna with a nonlinear load (in which a diode model consists of a parallel combination of a nonlinear resistance and a nonlinear junction capacitance along with a linear series inductance, a linear series resistance, and a linear package capacitance) has been carried out using a time-stepping finite difference equation technique along with the Newton–Raphson iteration method and will be presented in the future.

APPENDIX A

THE SOLUTION FOR A FIRST-ORDER NONLINEAR DIFFERENTIAL EQUATION

With the following substitution

$$y(t) \equiv \frac{1}{au(t)} \frac{du(t)}{dt}, \tag{A1}$$

(9) reduces to

$$\frac{d^2u(t)}{dt^2} + f\frac{du(t)}{dt} = 0 \equiv \frac{dw(t)}{dt} + fw(t), \tag{A2}$$

where

$$\frac{du(t)}{dt} \equiv w(t). \tag{A3}$$

The solution of (..2) is given by

$$\ln w(t) = -\int_0^t f(\tau)\, d\tau = bv_i(t) + at + c, \tag{A4}$$

where

$$b = \frac{\alpha}{1 + C_d/C_a}, \tag{A5}$$

$$a = \frac{\alpha I_s}{C_a + C_d}, \tag{A6}$$

and from the initial condition

$$c = 0. \tag{A7}$$

Then

$$y(t) \equiv e^{\alpha v_0(t)} \equiv \frac{1}{au(t)} \frac{du(t)}{dt} = \frac{e^{bv_i(t)+at}}{a\left[\int_0^t e^{bv_i(\tau)+a\tau}\, d\tau\right] + d}. \tag{A8}$$

Hence the detected output voltage $v_0(t)$ is given by

$$v_0(t) = \frac{bv_i(t)}{\alpha} - \frac{1}{\alpha} \ln\left[de^{-at} + ae^{-at}\int_0^t e^{bv_i(\tau)+a\tau}\, d\tau\right]. \tag{A9}$$

When the induced voltage $v_i(t)$ is a periodic sinusoid, i.e., $v_i(t) = V_i \sin \omega t$, the second term in the natural logarithms can be integrated analytically. The integration over a complete cycle becomes

$$\int_0^t e^{bv_i(\tau)+a\tau}\, d\tau = \sum_{n=0}^{[t/p]-1} e^{nap} \int_0^p e^{bv_i(\tau)+a\tau}\, d\tau$$

$$= \frac{1 - e^{[t/p]ap}}{1 - e^{ap}} \int_0^p e^{bv_i(\tau)+a\tau}\, d\tau$$

$$\equiv \frac{1 - e^{[t/p]ap}}{1 - e^{ap}} I, \tag{A10}$$

where p is the period, $[t/p]$ is the largest integer in t/p, and

$$I \equiv \int_0^p e^{bv_i(\tau)+a\tau} d\tau. \tag{A11}$$

By substituting (A10) into (A9),

$$v_0(t) = \frac{bv_i(t)}{\alpha} - \frac{1}{\alpha} \ln \left[\left(d + \frac{aI}{1 - e^{ap}} \right) e^{-at} + \frac{aI}{e^{ap} - 1} \right]. \tag{A12}$$

Note that the first term in the natural logarithms goes to zero for large positive t.

By taking a time average of $v_0(t)$ over a complete cycle, the detected dc voltage becomes

$$\overline{V_0} = -\frac{1}{\alpha} \ln \frac{aI}{e^{ap} - 1}, \tag{A13}$$

since

$$\overline{v_i(t)} = 0. \tag{A14}$$

Equation (A11) can be integrated analytically for a sinusoidal induced voltage $v_i(t) = V_i \sin \omega t$:

$$\begin{aligned} I &= \int_0^p e^{bV_i \sin \omega\tau + a\tau} \, d\tau \\ &= \omega^{-1} \int_{-\pi}^{\pi} e^{bV_i \sin(\tau' + \pi) + \frac{a(\tau' + \pi)}{\omega}} \, d\tau' \\ &= \omega^{-1} e^{\pi T} \int_{-\pi}^{\pi} e^{-bV_i \sin \tau' + T\tau'} \, d\tau' \\ &= 2\pi\omega^{-1} e^{\pi T} J_{jT}(jU), \end{aligned} \tag{A15}$$

where $J_{jT}(jU)$ is the Anger function of imaginary order (jT) and imaginary argument (jU), T is the normalized period

$$T = \frac{a}{\omega} = \frac{\alpha I_s}{\omega(C_a + C_d)}, \tag{A16}$$

and U is the normalized induced voltage

$$U = bV_i = \frac{\alpha V_i}{1 + C_d/C_a}. \tag{A17}$$

Substituting (A15) into (A13) the detected dc voltage average over a complete cycle becomes

$$\overline{V_0} = -\frac{1}{\alpha} \ln \frac{2\pi a e^{\pi T} J_{jT}(jU)}{\omega(e^{ap} - 1)} = -\frac{1}{\alpha} \ln \frac{\pi T J_{jT}(jU)}{\sinh \pi T} \tag{A18}$$

which is given in (12).

APPENDIX B

SERIES REPRESENTATION FOR THE DETECTED DC VOLTAGE

The detected dc voltage averaged over a complete cycle is given by (12)

$$\overline{V_0} = -\frac{1}{\alpha} \ln \frac{\pi T J_{jT}(jU)}{\sinh \pi T}. \tag{B1}$$

Using the series representation for the Anger function

$$J_\nu(z) = \frac{\sin \nu\pi}{\nu\pi} s_1(\nu, z) + \frac{\sin \nu\pi}{\pi} s_2(\nu, z), \tag{B2}$$

where

$$s_1(\nu, z) = 1 + \sum_{\substack{m=2 \\ \text{even}}}^{\infty} \frac{(-1)^{m/2} z^m}{\prod_{\substack{k=2 \\ \text{even}}}^{m} (k^2 - \nu^2)}, \tag{B3}$$

and

$$s_2(\nu, z) = \sum_{\substack{m=1 \\ \text{add}}}^{\infty} \frac{(-1)^{(m-1)/2} z^m}{\prod_{\substack{k=1 \\ \text{odd}}}^{m} (k^2 - \nu^2)}. \tag{B4}$$

Since

$$J_{jT}(jU) = \frac{\sinh \pi T}{\pi T} s_1(jT, jU) + \frac{j \sinh \pi T}{\pi} s_2(jT, jU), \tag{B5}$$

we have

$$\begin{aligned} \frac{\pi T J_{jT}(jU)}{\sinh \pi T} &= [s_1(jT, jU) + jTs_2(jT, jU)] \\ &\equiv S_1(T, U) - TS_2(T, U), \end{aligned} \tag{B6}$$

where

$$S_1(T, U) = 1 + \sum_{\substack{m=2 \\ \text{even}}}^{\infty} \frac{U^m}{\prod_{\substack{k=2 \\ \text{even}}}^{m} (k^2 + T^2)}, \tag{B7}$$

and

$$S_2(T, U) = \sum_{\substack{m=1 \\ \text{odd}}}^{\infty} \frac{U^m}{\prod_{\substack{k=1 \\ \text{odd}}}^{m} (k^2 + T^2)}. \tag{B8}$$

By substituting (B6) into (B1) the detected dc voltage averaged over a complete cycle becomes

$$\overline{V_0} = -\frac{1}{\alpha} \ln [S_1(T, U) - TS_2(T, U)]$$

which is given in (15).

APPENDIX C

HIGH-FREQUENCY APPROXIMATION

At high frequencies where

$$T = \frac{\alpha I_s}{\omega(C_a + C_d)} \ll 1, \tag{C1}$$

(16) and (17) are approximated as

$$S_1(T, U) \cong 1 + \frac{U^2}{2^2} + \frac{U^4}{2^2 4^2} + \cdots \tag{C2}$$

$$TS_2(T, U) \cong 0. \tag{C3}$$

For small V_i, i.e., small U, the detected dc voltage averaged over a complete cycle becomes

$$\begin{aligned} \bar{V}_0 &= -\frac{1}{\alpha} \ln [S_1(T, U) - TS_2(T, U)] \\ &\cong -\frac{1}{\alpha} \ln \left(1 + \frac{U^2}{2^2}\right) \\ &\cong -\frac{U^2}{4\alpha} = -\frac{\alpha}{4} \left[\frac{V_i}{1 + C_d/C_a}\right]^2 \end{aligned} \tag{C4}$$

which is given in (19). For large V_i, i.e., large U, the detected dc voltage averaged over a complete cycle becomes

$$\begin{aligned} \bar{V}_0 &= -\frac{1}{\alpha} \ln [S_1(T, U) - TS_2(T, U)] \\ &\cong -\frac{1}{\alpha} \ln \left(1 + \frac{U^2}{2^2} + \frac{U^4}{2^2 4^2} + \cdots\right) \\ &= -\frac{1}{\alpha} \ln I_0(U), \end{aligned} \tag{C5}$$

where $I_0(U)$ is the modified Bessel Function of zeroth order. Applying asymptotic expansion for $I_0(U)$ for large arguments U, the dc voltage becomes

$$\bar{V}_0 \cong -\frac{1}{\alpha} \ln \frac{e^U}{\sqrt{2\pi U}} \cong -\frac{U}{\alpha} = -\frac{V_i}{1 + C_d/C_a}, \tag{C6}$$

which is given in (20).

ACKNOWLEDGMENT

The author wishes to express his appreciation to P. F. Wacker, N. S. Nahman, M. T. Ma, R. R. Bowman, S. M. Riad, C. K. S. Miller, and F. X. Ries for many stimulating discussions and suggestions in the preparation of this paper.

REFERENCES

[1] P. F. Wacker and R. R. Bowman, "Quantifying hazardous electromagnetic fields: Scientific basis and practical considerations," *IEEE Trans. Microwave Theory Tech.*, vol. MTT-19, no. 2, pp. 178–187, Feb. 1971.

[2] N. Wiener, *Nonlinear Problems in Random Theory*. Cambridge, MA: Massachusetts Institute of Technology, 1959.

[3] T. K. Sarkar and D. D. Weiner, "Scattering analysis of nonlinearly loaded antennas," *IEEE Trans. Antennas Propagat.*, vol. AP-24, no. 2, pp. 125–131, Mar. 1976.

[4] H. Schuman, "Time-domain scattering from a nonlinearly loaded wire," *IEEE Trans. Antennas Propagat.*, vol. AP-22, pp. 611–613, July 1974.

[5] T. K. Liu and F. M. Tesche, "Analysis of antennas and scatterers with nonlinear loads," *IEEE Trans. Antennas Propagat.*, vol. AP-24, no. 2, pp. 131–139, Mar. 1976.

[6] T. K. Liu, F. M. Tesche, and F. J. Deadrick, "Transient excitation of an antenna with a nonlinear load: Numerical and experimental results," *IEEE Trans. Antennas Propagat.*, vol. AP-25, no. 4, pp. 539–541, July 1977.

[7] J. A. Landt, "A unified time-domain electromagnetic and circuit analysis code," 1977 USNC/URSI Meeting, Stanford, CA, p. 153, June 1977.

[8] M. Kanda, "The characteristics of broadband, isotropic, electric field and magnetic field probes," NBSIR 77-868, Nov. 1977.

[9] D. A. Calahan, *Computer-Aided Network Design*, rev. ed. New York: McGraw-Hill, 1972.

Motohisa Kanda (S'67–M'78) was born in Kanagawa, Japan, on September 10, 1943. He received the B.S. degree from Keio University, Tokyo, Japan, in 1966 and the M.S. and Ph.D. degrees in electrical engineering from the University of Colorado, Boulder, in 1968 and 1971, respectively.

From 1965 to 1966 he did research on the avalanche breakdown in the germanium p–n junction at cryogenic temperature at Keio University. From 1966 to 1971 he was a Research Assistant at the University of Colorado, where he was engaged in research on impact ionization of impurities in n-type germanium and nonreciprocal behavior in solid-state magnetoplasma at millimeter and submillimeter wavelengths. In 1971 he joined the staff of the Electromagnetic Fields Division, National Bureau of Standards, Boulder, CO, where he is presently engaged in developing systems and techniques for use in microwave noise measurements.

Dr. Kanda is a full member of Commissions A, B, and E of the International Union of Radio Science and Sigma Xi.